CO_2 reactivity on Fe–Zn–Cu–K Fischer–Tropsch synthesis catalysts with different K-loadings

Michela Martinelli[a], Carlo Giorgio Visconti[a,*], Luca Lietti[a], Pio Forzatti[a], Claudia Bassano[b], Paolo Deiana[b]

[a] *Politecnico di Milano, Dipartimento di Energia, Piazza Leonardo da Vinci 32, Milano 20133, Italy*
[b] *ENEA, Agenzia Nazionale per le Nuove Tecnologie, l'Energia e lo Sviluppo Economico Sostenibile, Via Anguillarese 301, S. Maria di Galeria, Roma 00123, Italy*

Received 17 July 2013
Received in revised form
12 November 2013
Accepted 15 November 2013
Available online 17 December 2013

1. Introduction

Carbon dioxide is the primary greenhouse gas (GHG) arising from life and human activities. In recent years, the growing consciousness of the dramatic impact of its atmospheric concentration on the climate has brought to conclusion that the reduction of CO_2 emissions from all anthropogenic processes is mandatory [1]. In addition to the improvement of the efficiency of energy conversion and utilization processes, GHG reduction strategies proposed in the last decades also include secondary measures such as the carbon dioxide capture and the storage (CCS). Apart from the open technological issues associated to these technologies, it has been recently shown that the costs related to the CO_2 re-injection are extremely high, thus making CCS hardly convenient even in the presence of carbon-emission taxes [2]. This paves the way to the so-called CO_2 capture and utilization (CCU) technologies, where it is no more considered as a waste to be dumped but is used as feedstock (C_1 building unit) to produce highly added-value products such as chemicals or fuels.

In addition to these carbon management strategies, the development of CO_2 utilization technologies being able to co-activate CO and CO_2 has become more and more strategic when considering that carbon dioxide is a significant component in syngas produced through natural gas partial oxidation, and steam reforming or through biomass gasification [3]. Until now, it is generally separated from CO/H_2 with important heat and energy loss [4].

* Corresponding author. Tel.: +39 0223993297; fax: +39 0223993318.
E-mail address: carlo.visconti@polimi.it (C.G. Visconti).

As a matter of fact, the most studied CO_2 conversion technologies involve its hydrogenation into chemicals or fuels [1,5] or the so called dry-reforming, i.e., its conversion to syngas *via* reaction with methane [6]. The major advantage to the use of CO_2 for the production of fuels is that their market is big enough to guarantee a relevant CO_2 consumption [7].

The processes under investigation to produce fuels from CO_2 can be divided into two main categories: *via* methanol and *via* modified Fischer–Tropsch synthesis (FTS). In the methanol-mediated approach, CO_2 is first converted to methanol over a Cu–Zn based catalyst, which is then transformed into hydrocarbons through a methanol to gasoline (MTG) process [1,8]. Methanol may be eventually dehydrated to dimethyl-ether, a valid alternative to diesel fuels. At variance, in the case of modified FTS, CO_2 is directly hydrogenated to linear hydrocarbons.

A number of studies are available where the direct hydrogenation of CO_2 and CO/CO_2 mixtures to hydrocarbons is reported on traditional FTS catalysts. In the case of cobalt-based catalysts (in the case of ruthenium as well [8]) there is a general consensus to the fact that carbon dioxide behaves as inert when CO is co-fed while the reaction regime shifts from a Fischer–Tropsch type to a methanation type when CO is completely replaced by CO_2 [9–16]. The reason of the different reactivity of CO and CO_2, however, is still debated, as it has been recently pointed out by Visconti et al. [10] and Gnanamani et al. [9]. In this respect, low temperature Fe-based catalysts are reported to be much more effective then cobalt to convert CO_2 to high molecular weight hydrocarbons. This is attributed either to the intrinsic reverse water gas shift (RWGS) activity of those catalysts [17], which is possibly the first step involved in the CO_2 conversion to hydrocarbons [18,19] or to their ability to directly hydrogenate carbon dioxide [20]. However, also in this case different evidences were collected by several groups and various explanations were used to justify the different reactivity of CO and CO_2. Riedel et al. [11], working with a $100Fe/13Al_2O_3/10Cu/10K$ (mass ratios) catalyst, found similar products as a result of CO and CO_2 hydrogenations, and explained this result by assuming that the carbides irreversibly formed during CO hydrogenation, which are responsible for the formation of the FT regime over Fe-based catalysts, can be formed even when CO_2 is fed. On the contrary, according to Gnanamani et al. [9], the C_{5+} selectivity drops significantly when switching from CO to CO_2 on a K-promoted Fe-catalyst (100Fe/4.4Si/0.9 K, atomic ratios). These authors explained such a result by assuming that due to the slow RWGS, the H_2/CO ratio in the reactor is higher when CO_2 is fed instead of CO. Similar results are also reported by Yao et al. [21] on a supported Fe/TiO_2 catalyst; a significant decrease of the olefin to paraffin (O/P) ratio is also observed when replacing CO with CO_2. Finally, Dwyer and Somorjai [22], and Ando et al. [23], working with unpromoted bulk iron catalysts, reported different product composition during the hydrogenation of CO and CO_2 with a shift to light and saturated hydrocarbons in the latter case. This has been explained by speculating that the formation of the active carbide species (χ-$Fe_{2.2}C$), readily occurring on the catalytic surface in the presence of CO, is suppressed in the presence of CO_2 [23]; the catalytic surface would be indeed oxidized during the conversion of CO_2 to CO.

The cofeeding of CO and CO_2 also leads to puzzling results. Xu et al. [24] and Yao et al. [21] found that CO_2 is hydrogenated only at low CO partial pressure due to a relevant contribution of the RWGS at these conditions. However, when CO_2 is converted, the selectivity to methane suddenly increases but decreases to C_{2+} hydrocarbons [21]. The same authors show that O/P ratio progressively decreases when CO is replaced by CO_2 [13]. At variance, Gnanamani et al. [9] reported similar (always very low) CO_2 conversions upon varying the CO/CO_2 feed ratio; also, the product distribution was found to depend only on the H_2/CO ratio, independently on the presence of CO_2. Chun et al. [4], working with a $100Fe/5.33Cu/5.23\,K/17.4SiO_2$ (mass ratios), found an inhibiting effect of CO_2 in terms of hydrocarbon yield; the carbon number distribution as well as the O/P ratio was however not affected. They attributed such a decrease to a competitive adsorption of CO and CO_2.

With the purpose to gain more insights on the reactivity of carbon dioxide on Fe-based catalysts, in this work, the catalytic performances of K-promoted 100Fe/10Zn/1Cu samples have been comparatively studied in the hydrogenation of CO, CO_2, and CO/CO_2 mixtures. The effect of potassium on the catalyst activity and selectivity has been investigated by reactivity of samples having different K-loadings. Due to the fact that Fe-based catalysts are usually considered for coal to liquid (CTL) and biomass to liquid (BTL) processes which operate with H_2-deficient synthesis gas ($H_2/CO \sim 1$ mol/mol), reactivity studies have been carried out in this work with equimolar H_2/CO and H_2/CO_2 mixtures, and results are shown in the following experiments .

2. Experimental

2.1. Catalyst preparation

Following the procedure reported in [25], potassium and copper promoted 100Fe/10Zn catalysts were prepared by semi-batch co-precipitation of ferric and zinc nitrates at constant pH to form porous Fe-Zn oxy/hydroxycarbonate powders, which were then promoted after calcination at 350 °C by incipient wetness impregnation with potassium carbonate and copper nitrate. Briefly, a ferric nitrate solution (3.0 M) and a zinc nitrate solution (1.4 M) were prepared by dissolving $Fe(NO_3)_3{\cdot}9H_2O$ (Aldrich, ≥98%) and $Zn(NO_3)_2{\cdot}6H_2O$ (Aldrich, ≥98%) in deionized water. The two solutions were then mixed so as to obtain a Zn/Fe atomic ratio of 0.1. The resulting solution was continuously fed to a jacketed glass reaction cell kept at 80 °C containing a buffer solution ($(NH_4)_2CO_3$ 1.0 M (Aldrich, ≥30% NH_3 basis) acidified at pH = 7 with nitric acid. This led to the co-precipitation of the Fe and Zn hydroxycarbonates. $(NH_4)_2CO_3$ 1.0 M was added to the cell through an electronic titrator (Metrohm, Titrino plus) to keep the pH of the slurry at a value of 7 ± 0.2.

The obtained slurry was filtered and the obtained solid was then washed five times with deionized water (500 cm^3 each time), dried in ambient air at 120 °C overnight and eventually calcined in stagnant ambient air at 350 °C for 1 h (heating rate 1 °C/min). Then, copper (Cu/Fe = 0.01 atomic ratio) and potassium (K/Fe = 0.02 or 0.04 atomic ratios) promoters were sequentially added to the Fe–Zn calcined precursor by the incipient wetness impregnation technique starting from aqueous solutions of $Cu(NO_3)_2{\cdot}3H_2O$ (Aldrich, >98%) and K_2CO_3 (Aldrich, ≥99%). After each impregnation steps, the samples were dried in ambient air at 120 °C overnight. After impregnation with potassium, samples were calcined at 400 °C in stagnant air for 4 h (heating rate 1 °C/min). This procedure led to the complete decomposition of all precursor salt except K_2CO_3.

Two catalysts, with different K-loadings, were prepared: 100Fe/10Zn/1Cu/2K (sample "cat2K") and 100Fe/10Zn/1Cu/4K (sample "cat4K") on a molar base.

2.2. Catalyst characterization

Both the precursors of "cat2K" and "cat4K" (named "prec2K" and "prec4K", respectively), i.e., the samples obtained after Fe–Zn co-precipitation and the final catalysts obtained after Cu–K impregnation ("cat2K" and "cat4K") were characterized.

Powder X-ray diffraction measurements were carried out using a D8 Advance Bruker diffractometer and Cu-Kα radiation

($\lambda = 1.54$ Å). The adopted scan rate was 12.5 s^{-1} and 2θ range was 10–80°.

BET surface area and pore volume were measured using a Micromeritics Tristar 3000 instrument and nitrogen physisorption at its normal boiling point after evacuating the samples at 120 °C overnight.

The extent of reduction of the catalysts was measured by a temperature programmed reduction (TPR) method using a Thermo Scientific TPDRO 1100 instrument. In a typical test 30 mg of powder catalyst were placed in a quartz reactor (9.6 mm i.d.) and first treated in 20 vol.% O_2 in Ar (Sapio) with a flow rate of 10 cm^3/min (at standard temperature and pressure, STP, 0 °C, 1 ata) by heating from ambient temperature to 400 °C at 10 °C/min, holding at 400 °C for 1 h, and then cooling to ambient temperature in He. The flow was then switched to 20 vol.% H_2 in Ar (Sapio) at 20 cm^3(STP)/min and the reactor temperature was increased to 1000 °C at 10 °C/min. Hydrogen consumption was quantified by an on-line thermal conductivity detector (TCD).

SEM-EDX measurements were carried out on a Zeiss Evo50 EP scanning electron microscope equipped with Oxford Inca Energy 200–Pentafet LZ4 energy dispersive X-ray spectrometer.

2.3. Catalyst testing

The reactivity of "cat2K" and "cat4K" in the presence of CO and/or CO_2 was tested by feeding the reactor with $CO/H_2/Ar$ (31/67/2 v/v, Sapio), $CO/H_2/N_2$ (32/32/36 v/v, Sapio), $CO_2/H_2/N_2$ (32/32/36 v/v, Sapio) and $CO/H_2/CO_2/Ar$ (32/32/32/4 v/v, Sapio) mixtures keeping the other process conditions constant ($T = 220$ °C, $P = 30$ bar, GHSV = 6000 cm^3(STP)/h/g_{cat}).

Activity tests were carried out in a lab-scale plant equipped with a fixed-bed reactor placed into a home-made electric furnace. The reacting mixture was purified by potentially contained iron carbonyls and then fed to the reactor (i.d. = 1.1 cm, length = 85 cm) by means of a single mass flow controller (Brooks Instrument, SLA5850). The unconverted gas and the reaction products leaving the reactor were send to a hot vessel heated to 110 °C for the collection of the waxes. The transfer lines from the reactor to the trap and from the trap to the on-line GC were kept at 150 °C to prevent the condensation of the reaction products. The reactor pressure was controlled using a home-made dome-load regulator.

Reactants and gaseous products were periodically analyzed using an on-line gas chromatograph (Agilent, 7820 A) equipped with four columns, and two detectors. A first column (Agilent, HayeSep Q 80/100 mesh, length = 0.91 m, i.d. = 2 mm,) was used to cut permanent gases from hydrocarbons. H_2, N_2, and CO (and eventually CH_4) were sent in a molecular sieve packed column (Agilent, MolSieve 13X 60/80 mesh, length = 3.05 m, i.d. = 2 mm,) connected to a thermal conductivity detector while CO_2 was separated through a HayeSep Q packed column (Agilent, HayeSep Q 80/100 mesh, length = 1.83 m, i.d. = 2 mm) also connected to the thermal conductivity detector. C_1–C_{10} hydrocarbons were instead separated in a KCl/Al_2O_3 plot capillary column (Agilent, CP-Al_2O_3/KCl PT, 25 m × 0.53 mm × 10 μm), and quantified through a flame ionization detector. N_2 or Ar has been used as internal standards during GC analysis.

The waxes, periodically collected from the hot trap, were analyzed by an off-line gas-chromatograph (Hewlett-Packard, 6890) equipped with one flamed ionization detector, one capillary column (Agilent J&W HP-5, 30 m × 0.32 mm × 0.25 μm), and one on-column injector. The waxes, solid at room temperature, were dissolved in CS_2 before injection.

Such procedures allowed us to quantify C_1–C_{46} paraffins and C_2–C_{26} olefins. Organic oxygenates, which accounted for less than 15% of consumed CO and CO_2, were neglected. Due to the layout of our experimental apparatus, in particular the product condensation section, a fraction of C_{11}–C_{15} species were lost during waxes collection, possibly being solubilized in the liquid waxes. Accordingly, their quantification was considered unattainable and selectivity data referring to those species will not be plotted nor discussed in this paper.

In a typical run, the catalyst (0.5 g), diluted with α-Al_2O_3 (1:10 v/v), was loaded in the reactor and reduced/activated in situ at 270 °C (heating ramp = 1 °C/min) for 1 h, feeding syngas ($H_2/CO = 2$ mol/mol, GHSV = 6000 cm^3(STP)/h/g_{cat}) at atmospheric pressure [25]. Then, the reactor was cooled down to 220 °C and slowly pressurized at 30 bar. Process conditions were thus kept unchanged until both the CO conversion rate and the product distribution reached a steady state.

Carbon selectivity to the i-species (S_i) has been calculated according to Eq. (1):

$$S_i = \frac{F_i^{out} \times n_i}{F_{CO}^{in} \times \chi_{CO} + F_{CO_2}^{in} \times \chi_{CO_2}} \quad (1)$$

where, F_i^{out} is the molar productivity of i-hydrocarbon species, n_i is the carbon number, F_{CO}^{in} is the CO inlet molar flow, $F_{CO_2}^{in}$ is the CO_2 inlet molar flow, χ_{CO} is the CO conversion, and χ_{CO_2} is the CO_2 conversion.

Table 1
Textual proprieties of prepared materials.

Sample tag	Surface area [m^2/g]	Pore volume [cm^3/g]	Average pore diameter [Å]
"prec2K"	159	0.25	48
"cat2K"	76	0.21	90
"prec4K"	154	0.25	48
"cat4K"	85	0.20	75

3. Results and discussion

3.1. Catalysts characterization

"prec2K" and "prec4K" precursors which have the same nominal composition were prepared in two replicated batches by following the procedure described in Section 2.1. XRD analyses (Fig. 1(a)) showed the presence in both the samples of microcrystalline α-Fe_2O_3 (hematite) and $ZnFe_2O_4$ (zinc ferrite). The two samples have similar textural properties (Table 1).

"cat2K" and "cat4K" are more crystalline than the corresponding precursors (Fig. 1(b)), especially in the case of the sample with the lowest K-loading ("cat2K"). More specifically, XRD patterns show, in both the samples, sharp peaks which are associated to a crystalline α-Fe_2O_3 phase. The zinc ferrite spinel phase ($ZnFe_2O_4$), on the contrary, remains microcrystalline. Such a result demonstrates an effect of potassium on the catalyst structural characteristics and is in line with literature data showing the crystallization of $ZnFe_2O_4$ around 400 °C for K-free Fe:Zn catalysts [26]. The average size of crystalline α-Fe_2O_3 particles, calculated by Scherrer formula using the peak at $2\theta = 49.6°$ is 23 nm for "cat2K" and 20 nm for "cat4K" indicating a slight effect of the potassium content on the crystal size of the samples. No peaks associated with potassium and copper phases have been detected by XRD possibly because of their low concentrations and the good dispersion.

As a result of the higher crystallinity of the final catalysts, these samples show a lower specific surface area and bigger average pore size than the precursors, 76 m^2/g with 90 Å pores for "cat2K" and 85 m^2/g with 75 Å pores for "cat4K" (Table 1 and Fig. 2). The higher specific surface area of "cat4K" with respect to "cat2K" is in line with its lower crystallinity.

A significant effect of potassium loading on the textural properties of iron-based FT catalysts has been also reported by Yan et al.

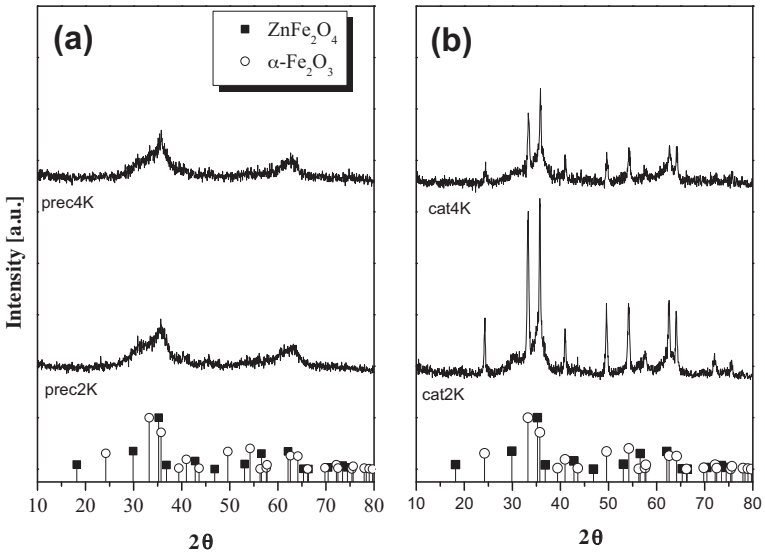

Fig. 1. XRD patterns for (a) the precursors and (b) the final catalysts with different potassium loading.

[27]. By characterizing samples with different K-loadings, they have found a maximum value of the surface area for a K/Fe weight ratio of 0.06. At variance, Yang et al. [28], and Lohitharn and Goodwin [29] observed a loss of surface area by increasing the alkali content in potassium promoted iron-manganese catalysts. Wan et al. [30] proposed that the addition of potassium enhances the aggregation of Fe-crystallites, thus resulting in a decrease of the surface area. The discrepancy between data reported in [28–30] and the data of this work could be ascribed to the different preparation procedure. In this work, potassium was added to the catalyst after calcination at 350 °C; such thermal treatment may induce the transformation of the iron oxy/hydroxycarbonates obtained during the co-precipitation into a more stable oxide phase, which is rather stable during the second calcination (at 400 °C) in the presence of potassium. At variance in the case of papers [28–30], potassium was added prior to the thermal treatments at high temperature, i.e., directly impregnating the dried precursors.

SEM micrographs of "cat2K" and "cat4K" samples are shown in Figs. 3 and 4(a). EDX mapping was used to analyze the Fe, Zn, Cu, K elemental distribution on the surface of the two samples (Figs. 3(b–e) and 4(b–e)); potassium and copper appear to be well distributed on the surface of both the catalysts with no evident segregation (at least at the micron-scale).

Finally, Fig. 5 shows the TPR profiles of "cat2K" and "cat4K" samples; two separate reduction peaks, one at temperatures below 300 °C and the other at temperatures below 700 °C, are visible for both the samples suggesting that the reduction mechanism occurs in two main steps for both the catalysts. According to the literature [25,29], the first peak corresponds to the reduction of α-Fe_2O_3 to Fe_3O_4 (partial reduction of Fe^{3+} to Fe^{2+}, Eq. (2)), whereas the second peak corresponds to the reduction of Fe_3O_4 to metallic iron (Eq. (4)). However, this latter step is expected to be rather complex because it involves the transformation of a mixture of Fe^{3+} and Fe^{2+} to Fe^0 which possibly occurs through the formation of a labile FeO species. Moreover, our catalysts also contain $ZnFe_2O_4$, whose reduction is reported to proceed through a series of steps involving at first its reduction to Fe_3O_4 and ZnO (Eq. (3)) and then the stepwise reduction of Fe_3O_4 to FeO and of FeO to metallic iron (Eq. (4)) [31]. Upon neglecting the fast transformation of FeO to Fe^0 [32], the reduction reactions for the prepared samples can be described by the following overall stoichiometries:

$$3\alpha\text{-}Fe_2O_3 + H_2 \rightarrow 2Fe_3O_4 + H_2O \quad (2)$$

$$3ZnFe_2O_4 + H_2 \rightarrow 2Fe_3O_4 + H_2O + 3ZnO \quad (3)$$

$$Fe_3O_4 + 4H_2 \rightarrow 3Fe^0 + 4H_2O \quad (4)$$

Based on the H_2 consumption measured in each of the two peaks of Fig. 5 and considering the stoichiometry of Eqs. (2)–(4), we assign the first peak (corresponding to a H_2 consumption of 0.17 $mol_{H2}/h/g_{Fe}$ for "cat2K" and 0.13 $mol_{H2}/h/g_{Fe}$ for "cat4K") to the reduction of hematite and zinc ferrite to magnetite (Eqs. (2) and (3)), and the second peak (1.35 $mol_{H2}/h/g_{Fe}$ for "cat2K" and 1.4 $mol_{H2}/h/g_{Fe}$ for "cat4K") to the conversion of magnetite to metallic iron (Eq. (4)).

Notably, TPR profiles clearly indicate that potassium shift at higher temperatures both the steps involved in the catalyst reduction process. In particular, by increasing the K/Fe atomic ratio from 0.02 to 0.04, the first reduction peak is shifted from 200 to 230 °C, while the second peak is shifted from 550 to 620 °C. Temperature programmed, and isothermal reduction studies conducted by Li [33] and Lohitharn et al. [29] also revealed that potassium inhibits the iron oxides reduction. Potassium is indeed an electron donor and its strong interaction with iron oxide suppresses the hydrogen adsorption on the catalyst surface, thus restraining the reduction of iron oxide particles underlying and/or neighboring the potassium promoter.

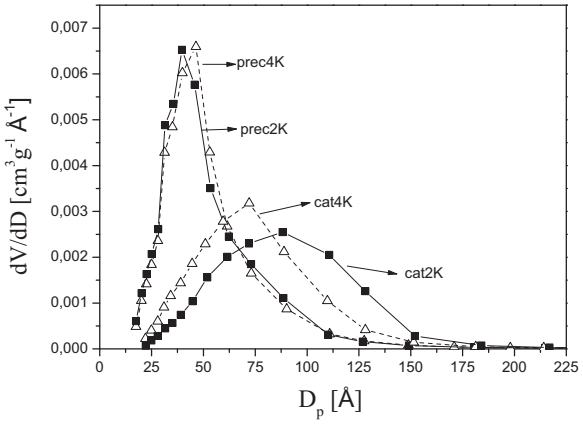

Fig. 2. Pore size distribution for the prepared samples.

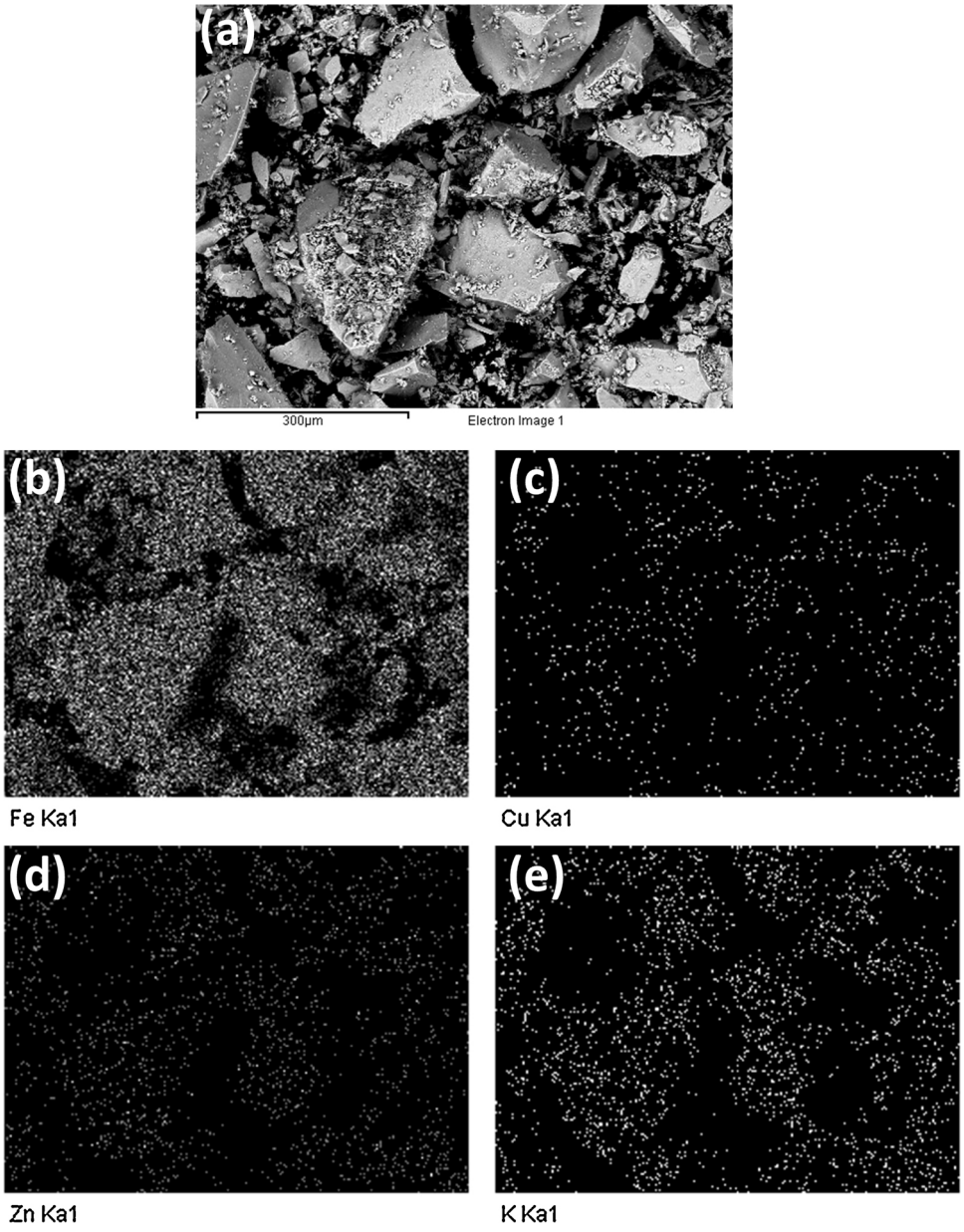

Fig. 3. EDX mapping of the surface of the "cat2K" sample.

3.2. Catalyst activity tests over 100Fe/10Zn/1Cu/2K catalyst ("cat2K")

The evolution of the CO conversion with time on stream (T.o.S.) is shown in Fig. 6 during "cat2K" stabilization phase, where the reactor was fed with syngas with $H_2/CO = 2$ until it reached steady-state conditions. "cat2K" initial activity grants a CO conversion higher than 30%; however, the catalyst progressively deactivates in the first hours reaching a CO conversion value of about 20% after 115 h on stream. Interestingly, the product selectivity does not change significantly in that period of time; CO_2 selectivity is around 19.8%, while CH_4 and C_{5+} selectivities are around 3.6% and 33.5%, respectively.

Similar evidences are reported in the literature [34,35] for 100Fe/0.3Cu/0.8K and 100Fe/5Zn (molar ratio) catalysts, which progressively deactivate in the first hours on stream in the presence of syngas. Such a behavior is typically attributed to carbon deposition which results into active sites blocking [34]. In this regard, it has to be noted that CO decomposition, which brings to the formation of superficial carbon (C_s) species, is necessary for the Fischer–Tropsch reaction to occur. Indeed, C_s species are responsible both for the catalytically active phase formation, which is known to be constituted by iron carbides and for the formation of the chain growth monomer (an adsorbed CH_x species) as a result of a stepwise hydrogenation process. The deposition of inactive carbon species (generally referred to as the Boudard reaction), the formation of bulk and surface iron carbides, and the formation of the chain growth monomer are three competitive processes whose relative rates are affected by many parameters such as the catalyst formulation (e.g., the surface basicity [36]), the process conditions (e.g., the H_2/CO ratio [34]), and the actual iron phase/oxidation number (oxide vs. metal vs. carbide).

Our data do not allow proving whether carbon deposition is the phenomenon controlling initial catalyst deactivation. However, the evidence that process selectivity is not affected by deactivation may be consistent with an unselective deactivation mechanism which brings to the gradual decrease of the number of active sites but does not affect the reactivity of the remaining sites.

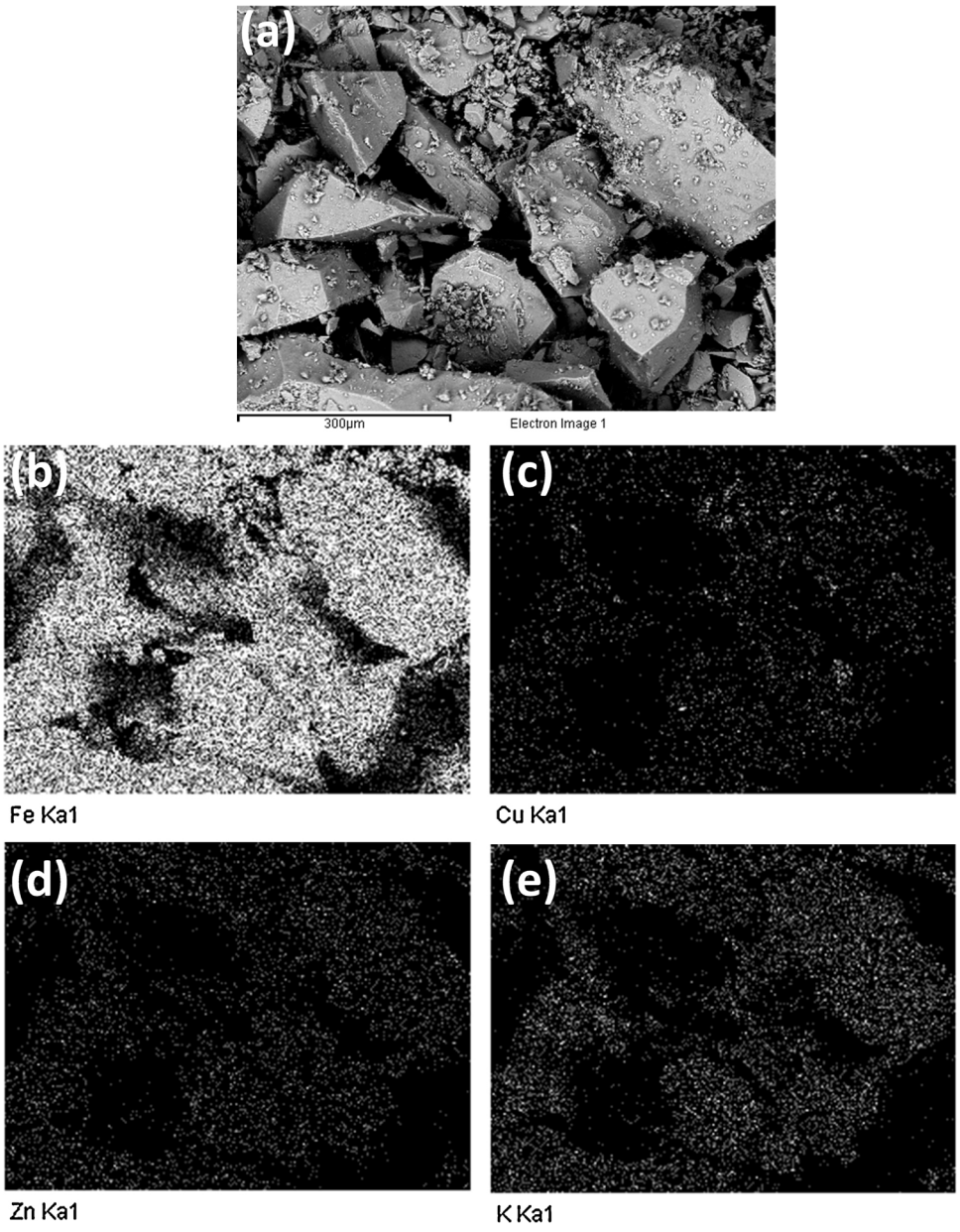

Fig. 4. EDX mapping of the surface for the "cat4K" sample.

3.2.1. Reactivity of $CO/H_2/N_2$ vs. $CO_2/H_2/N_2$

Steady state CO, CO_2, and H_2 conversion values measured in the test conditions #1 and #2 (Table 2), at time on stream higher than 115 h (i.e., at the end of the catalyst initial stabilization), are reported in Table 3. Over "cat2K", CO conversion is 14.1% while CO_2 conversion is 8.9%. Hydrogen consumption is higher in the case of CO hydrogenation (H_2 conversion = 21.4%) than in the case of CO_2 hydrogenation (16.1%). Accordingly, both CO and CO_2 are activated on the 100Fe/10Zn/1Cu/2K catalyst but CO_2 is less reactive than CO. These results are in agreement with those published in literature on both unpromoted [18] and promoted iron based catalysts [9,11].

The yields of the main reaction products (paraffins, olefins, and total hydrocarbons) are shown in Fig. 7 for the test conditions #1

Table 2
Process conditions adopted in CO, CO_2 and CO/CO_2 hydrogenation tests.

Condition number	#1	#2	# 3
Condition tag	$CO/H_2/N_2$	$CO_2/H_2/N_2$	$CO/H_2/CO_2$
T [°C]	220	220	220
GHSV [$cm^3(STP)h^{-1}g_{cat}^{-1}$]	6000	6000	6000
P [bar]	30	30	30
P^0_{H2} [bar]	9.6	9.6	9.6
P^0_{CO} [bar]	9.6	–	9.6
P^0_{CO2} [bar]	–	9.6	9.6
P^0_{N2} [bar]	10.8	10.8	–
P^0_{Ar} [bar]	–	–	1.2

Table 3
Conversion and selectivity values measured during tests at process conditions of Table 2.

Sample Tag	"cat2K"			"cat4K"		
Condition number	#1	#2	# 3	#1	#2	# 3
CO conversion [%]	14.1	–	10.5	7.9	–	7.5
CO_2 conversion [%]	–	8.9	2.7	–	8.3	2.1
H_2 conversion [%]	21.4	16.1	25.8	14.6	12.6	22.3
CO selectivity [%]	–	19.5	–	–	30.3	–
CO_2 selectivity [%]	28.8	–	–	32.0	–	–

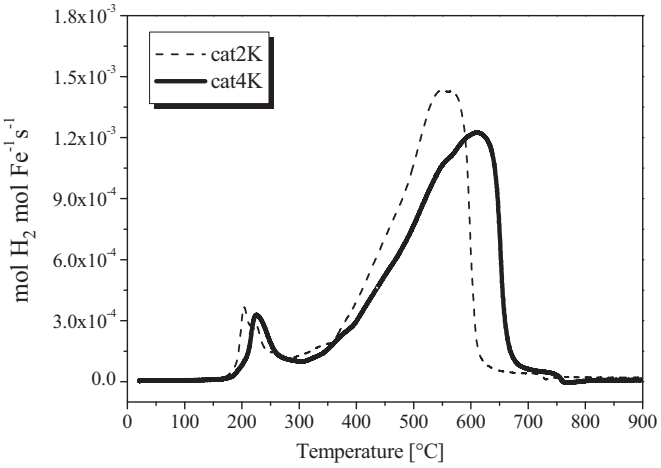

Fig. 5. H_2-TPR profiles for "cat2K" and "cat4K" samples (0.3 g).

and #2. In the case of CO hydrogenation, the paraffin specific yield (Fig. 7(a)) shows a complex trend as function of the carbon number (n). In fact the paraffin distribution initially decreases with the carbon number reaching a minimum in correspondence of $n = 9$, then it increases showing a maximum for $n = 17$ and eventually decreases again up to C_{46}. Anomalous are the behaviors of methane, which is by far the most abundant alkane, and of ethane, whose productivity is lower than that expected. The yield to C_{11}–C_{15} paraffins could not be estimated due to the reasons detailed above. Olefin specific yield (Fig. 7(b)) shows a decreasing trend with growing carbon number with ethylene out of trend due to its high reactivity in the presence of hydrogen [11]. The total hydrocarbon yield (Figure 7(c)) is characterized by two different trends: at low molecular weight, the olefins control the trend, while at high carbon numbers ($n > 10$) the trend is controlled by paraffins.

In the case of CO_2 hydrogenation, the product distribution is dramatically different from the previous case. The yield to light paraffins strongly increases (Fig. 7(a)) so that, for example, the yield to methane during CO_2 hydrogenation is about 4 times higher than that obtained in the case of CO hydrogenation and that of ethane is 7 times higher. On the contrary, C_{10+} paraffins are no more identified in the products pool. As opposite to paraffins, olefins show the same qualitative trend observed in the case of CO hydrogenation but their content in the products pool is lower (Fig. 7(b)). As a result, in the case of CO_2 hydrogenation tests, the total hydrocarbon yield is dominated by that of paraffins (Fig. 6(c)). This result differs from

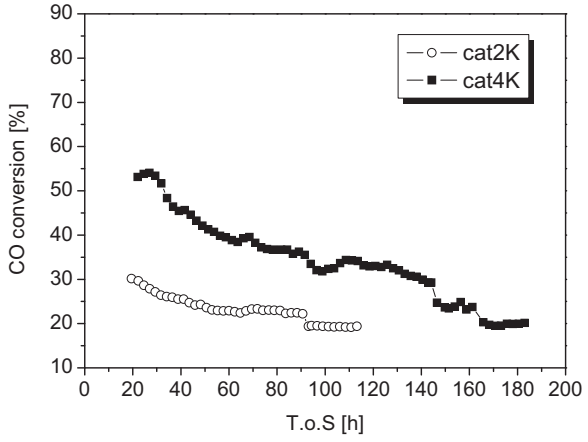

Fig. 6. CO conversion as a function of the time on stream for "cat2K" and "cat4K" samples (220 °C, 30 bar, 6000 cm^3(STP)/h/g_{cat}, H_2/CO = 2).

those reported by Riedel et al. [11,20], who on highly loaded potassium catalyst samples pointed out only marginal effects of the CO_2 feed on the selectivity and on the distribution of olefins.

The higher content of saturated hydrocarbons in the CO_2 hydrogenation [21,23] is further pointed out by olefin to paraffin molar ratios shown in Fig. 8 as a function of the carbon number. Indeed, during CO hydrogenation, olefins are the most abundant species ($O/P > 1$) until $n = 15$. At variance, during CO_2 hydrogenation, O/P ratio is always well below 1, and the trend as a function of n is characterized by a maximum for $n = 4$. It is speculated that the absence of liquid waxes filling the catalyst pores during CO_2 hydrogenation may be responsible for the peculiar reactivity of C_2–C_4 olefins. Indeed, in the case of cobalt based FT catalysts, it has been reported that the O/P trend is controlled by the increasing solubility of the olefins in the liquid waxes filling the catalysts pores as a function of their carbon number [37,38]

To complete the analysis of the O/P ratio, it is interesting to consider the olefins isomer distribution. As proposed by Riedel et al. [16], indeed, two types of catalytic sites may exist on promoted iron based FT catalysts. One group of sites would be responsible for the chain growth process and the formation of primary products, the other group would be responsible for olefin readsorption, double bond shift and secondary olefin hydrogenation. Accordingly, the ratio between terminal (primary) and internal (secondary) olefins is indicative of the presence of sites able to activate secondary olefin reactions [16]. The analysis of the distribution of the C_4 olefin isomers indentified in the product pool reveals that in both the case of CO and CO_2 hydrogenation tests previously described, α-olefins account for about 90% of the total butenes. Such a result, which is in line with the data collected by Riedel et al. [16] during both CO and CO_2 hydrogenation, is an evidence that both the groups of sites do exist on the catalytic surface of our samples, but indicates that secondary reactions are slow both in the case of CO and CO_2 hydrogenation processes, when the FT regime (i.e., the chain growth process) is largely dominant.

The total hydrocarbon product distribution obtained during CO and CO_2 hydrogenation are shown in Fig. 9 as per the terms of Anderson–Schulz–Flory (ASF) plots. In the case of CO hydrogenation, the ASF product distribution is characterized by two chain growth probability values α [39,40], with C_1 and C_2 out of trend. The estimated chain growth probabilities (α_1 and α_2) are equal to 0.63 for the hydrocarbons in the range C_3–C_7 (α_1) and equal to 0.89 for C_7–C_{50} hydrocarbons (α_2). A different picture is apparent in the case of CO_2 hydrogenation which does lead to an ASF product distribution characterized by a much lower α value (0.56) [41].

Interestingly, during CO hydrogenation, CO_2 is detected among the products with carbon selectivity near 29% (Table 3). At the same time, in the case of CO_2 hydrogenation, CO is found in the products pool, with carbon selectivity near 20%. These results indicate that the adopted catalyst, besides being able to hydrogenate CO to methane (Eq. (5)) and C_{2+} hydrocarbons (Eq. (6)), is also active in both the water gas shift and the reverse water gas shift processes (Eq. (7)).

$$\text{Methanation}: CO + 3H_2 \rightarrow CH_4 + H_2O \quad (5)$$

$$\text{Fischer–Tropsch}: CO + 2H_2 \rightarrow -CH_2- + H_2O \quad (6)$$

$$\text{Watergasshift}: CO + H_2O \rightarrow CO_2 + H_2 \quad (7)$$

Starting from the experimental CO_2 and CH_4 outlet molar flows, and from the moles of CO consumed in the process, the extent of reactions (5)–(7), namely ξ_5, ξ_6, and ξ_7, can be computed; during CO hydrogenation their values are 0.1152, 4.212, and 1.764 mmol/h, respectively. Accordingly, in the presence of a CO/H_2 feed stream, the Fischer–Tropsch process is dominant on the adopted catalyst, followed by water gas shift, and by the methanation.

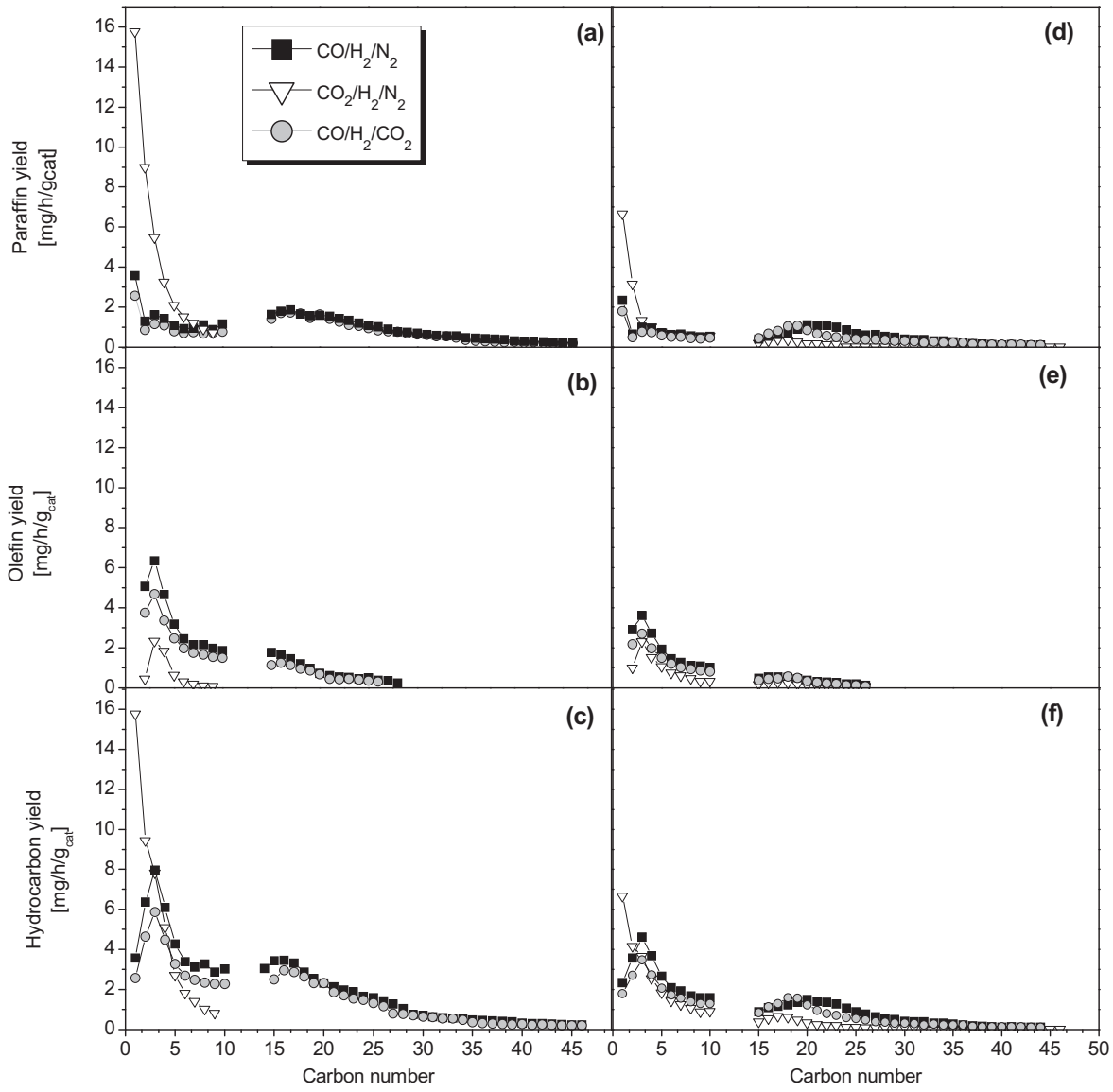

Fig. 7. (a) C_1–C_{46} paraffin yield; (b) C_2–C_{26} olefin yield; (c) total hydrocarbon yield during CO_x mixture hydrogenation on "cat2K". (d) C_1–C_{46} paraffin yield; (e) C_2–C_{27} olefin yield; (f) total hydrocarbon yield during CO_x mixture hydrogenation on "cat4K". Experimental conditions as in Table 2.

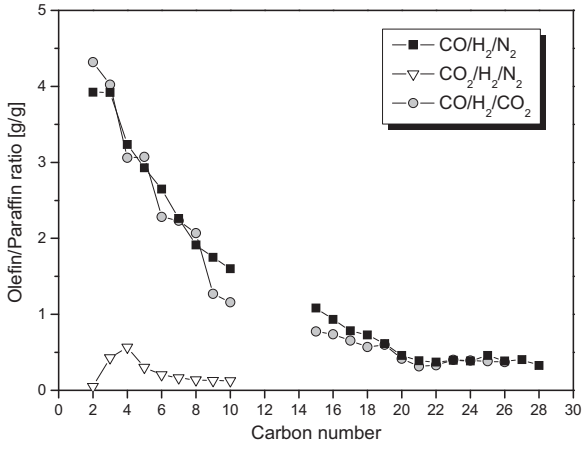

Fig. 8. O/P ratio during CO_x hydrogenation ("cat2K", experimental conditions as in Table 2).

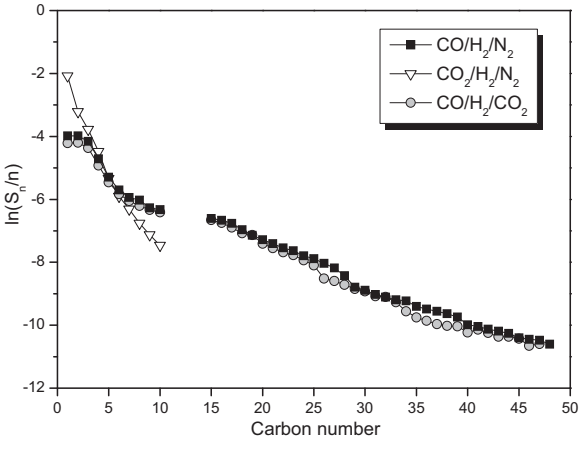

Fig. 9. ASF plots during CO_x hydrogenation ("cat2K", experimental conditions as in Table 2).

In the case of CO_2 hydrogenation, starting from the experimental values of CO and CH_4 outlet molar flows and from the moles of CO_2 consumed in the process, the following values of the extent of reactions (5)–(7) can be computed: 0.5040, 2.592, −3.888 mmol/h. In this case, the reverse water gas shift is dominant, followed by CO conversion to C_{2+} hydrocarbons and to CH_4. As expected by the higher CH_4 selectivity obtained in the case of CO_2 hydrogenation, ξ_6/ξ_5 for CO_2 hydrogenation (=5.1) is lower than that for CO hydrogenation (=36.6).

The lower chain growth probability [9,40] and the higher content of saturated hydrocarbons [21,23] obtained during CO_2 hydrogenation point out that hydrogenation reactions are more important when CO is replaced by CO_2. Under severe hydrogenating conditions, indeed, the chain termination reaction via hydrogenation (leading to light paraffins) becomes faster than both the chain growth reaction (leading to heavy hydrocarbons) and the β-hydride elimination reaction (leading to desorption of the growing hydrocarbon as olefin) [42]. At the same time, however, it is noted that CO_2 hydrogenation is slower than CO hydrogenation. In line with the explanation proposed by Miller et al. [43], which observed similar effects, it is speculated that CO_2, as opposite to CO, is weakly adsorbed on the catalytic surface. As a result, the local H/C ratio is higher and the growing intermediates are more easily hydrogenated. The low CO_2 coverage, however, results in a lower CO_2 conversion rate, due to the lacking carbon sources on the surface.

3.2.2. Reactivity of $CO/H_2/N_2$ and $CO_2/H_2/N_2$ vs.$CO/H_2/CO_2$

Once verified the ability of the iron-based catalyst to hydrogenate CO_2 under the typical low-temperature FT process conditions, the reactivity of carbon dioxide in the presence of CO has been also evaluated. For this purpose, the reactivity of the catalyst in the presence of a $CO/H_2/CO_2$/Ar mixture (condition #3 in Table 2) has been investigated and compared to that measured in the presence of $CO/H_2/N_2$ and $CO_2/H_2/N_2$ mixtures (conditions #1 and #2, Table 2).

When CO and CO_2 are cofed to the catalyst, the CO conversion is about 10.5% and that of CO_2 is about 2.7% (Table 3). Hydrogen conversion is instead 25.8%. Interestingly, the CO conversion is lower than that (14.1%) measured with the $CO/H_2/N_2$ mixture, while the H_2 conversion is higher. At the same time, the very low CO_2 conversion indicates that the net WGS reaction rate is negligible at the adopted conditions. This is not due to thermodynamic reasons; at the adopted process conditions, the reacting system is indeed very far from the equilibrium and the WGS reaction is thermodynamically favored. Accordingly, CO_2 cofeeding inhibits the rate of the water gas shift reaction. As a result, when replacing N_2 with CO_2, CO conversion decreases because CO is no more converted to CO_2, while H_2 conversion increases because H_2 is no more produced through the WGS reaction.

The very low CO_2 conversion in the presence of CO (CO/CO_2 inlet molar ratio = 1) is in agreement with data reported in literature [11,21] according to which CO_2 behaves as inert at $CO_2/(CO + CO_2)$ ratios lower than 0.5–0.7.

Interestingly, the moles of CO converted into hydrocarbons at test conditions #1 and #3 is almost identical (4.3 mmol/h in condition #1 and 4.5 mmol/h in conditions #3), and both the ASF and the *O*/*P* plots for conditions #1 and #3, shown in Figs. 8 and 9 are almost perfectly superimposed. According to this result, no relevant inhibiting or promoting effects on the rate of CO conversion to hydrocarbons can be assigned to CO_2 [6]

A slightly negative CO_2 effect on the hydrocarbon formation rate was found by Chun et al. [44] in a $100Fe/5.33Cu/5.23K/17.4SiO_2$ (weight ratios) catalyst. A possible explanation for these latter results is the different catalyst structural promoter (SiO_2 is used by Chun et al. [44] instead of Zn) and the different K-loading.

On the other hand, carbon dioxide plays a role on the occurrence of the WGS reaction; indeed, in the presence of CO_2, the CO conversion via the WGS reaction is decreased. The possibility to inhibit the WGS reaction (i.e., the CO conversion to CO_2) by CO_2-cofeeding is extremely interesting in view of the fact that in principle, the reaction can be carried out with no net formation of CO_2, and hence with complete selectivity to hydrocarbons. Nevertheless, it has to be considered that WGS reaction is responsible for the consumption of part of the water produced during the hydrocarbon synthesis through reactions (5) and (6), and water is well known to inhibit the kinetics of hydrocarbon formation on Fe-based FT catalysts especially at low H_2/CO feed ratio and high CO conversion [45]. As a consequence, any effort aimed at reducing the amount of CO_2 produced during CO hydrogenation would negatively affect the hydrocarbon formation rate also. In order to take advantage from the beneficial effects of CO_2, the optimum concentration of CO_2 in the feed must be found able to grant the maximum yield to hydrocarbons defined as the moles of carbon converted to hydrocarbons divided by the moles of CO converted.

3.3. Catalyst activity tests over 100Fe/10Zn/1Cu/4K catalyst ("cat4K")

Following the results of Sections 3.2.1 and 3.2.2, the low adsorption strength of CO_2 is responsible for the low activity and the low chain growth probability measured in the presence of $CO_2/H_2/N_2$ mixtures as well as for its chemical inertia in the presence of equimolar amounts of CO. In order to promote CO_2 conversion to hydrocarbons is thus fundamental to find a way to promote the CO_2 adsorption strength. Due to the acidic nature of CO_2 (electron acceptor, Lewis acid), alkali-promoters are expected to favor the interaction between CO_2 and the catalyst. Accordingly, we repeated the CO, CO_2, and CO/CO_2 hydrogenation experiments (Table 2) on a catalyst with a double K loading ("cat4K", K/Fe = 4 mol. %).

In Fig. 6, the evolution of the CO conversion with T.o.S. is shown during "cat4K" stabilization phase. Initial activity for "cat4K" is significantly higher than for "cat2K", suggesting a promoting effect of potassium. However, CO conversion rapidly decreases in the first 180 h on stream, reaching a stable CO conversion value of about 20%, which is lower than that shown by "cat2K". Such a result, which is in line with the promotion role of potassium on CO conversion reported in the literature, is also compatible with a role of potassium in accelerating the catalyst deactivation, possibly through a promoting effect on the deposition of inactive carbon on the catalyst surface [34].

As in the case of cat2K, the reactivity of cat4K has been assessed only after the end of the initial stabilization phase, which for such catalyst corresponds to 180 h on stream (vs. 115 h of cat2K).

3.3.1. Reactivity of $CO/H_2/N_2$

In the case of CO hydrogenation, upon increasing the K/Fe ratio from 2 to 4 mol. %, the CO conversion decreases from 14.1 to 7.9% (Table 3) while the hydrogen conversion decreases from 21.4 to 14.6%.

Several studies have been carried out to investigate the effect of potassium on the CO hydrogenation activity over various iron-based catalysts under different reaction conditions [28,43,46–48]. In all the papers, it is reported that CO conversion shows a maximum as a function of the potassium content and the optimal potassium loading depends on the catalyst formulation. For example, Yang et al. [28] observed, in the case of Fe/Mn catalysts, a maximum activity in correspondence of a K loading near 0.7 wt.% while Raje et al. [46], who investigated co-precipitated K-promoted $100Fe/4.6SiO_2$ catalysts, observed the highest syngas conversion in

correspondence to a K/Fe ratio equal to 1.4 mol. %. Bukur et al. [47] found that catalyst activity increases significantly with increasing potassium loading up to K-contents of 0.5 wt. % but then it levels off for loadings of up to 1 wt.%. Miller and Moskovits [43], working with K-promoted electrodeposited Fe/Al catalysts, found the highest syngas conversion for the catalyst with a 2.8 wt.% K-loading. In line with these results, our data are possibly "beyond the maximum" in the region where the catalyst activity decreases upon increasing K-loading.

The lower CO conversion at high potassium loadings has been reported to be possibly due to the pore-blocking induced by poorly dispersed K clusters occurring already at K-loading as high as 0.3 wt% [48]. However, our SEM data seem to rule out this possibility at least for K/Fe ratios between 2 and 4 mol.%. Another explanation, which is frequently taken into account but which has never been proved, is that the increased carbon deposition promoted by high potassium loadings leads to the formation of inactive carbon covering the surface which suppresses the FTS activity [47]. The last explanation is based on the different effect of potassium loading on the CO and H_2 adsorption [43]. In fact, at the lowest K-loadings, H_2 chemisorption is stronger than CO dissociative chemisorptions. Accordingly, (i) the surface concentration of C_1 monomers is lower than that of H_2, and short chain hydrocarbons are favored since chain termination process can compete effectively with chain growth; (ii) the catalyst activity is limited due to the lacking carbon sources on the surface. Upon increasing the K loading, CO chemisorption is enhanced while H_2 chemisorption is progressively suppressed; at moderate K-levels, this effect boosts the catalyst activity and promotes the chain growth process and at higher K-levels on the contrary, strong CO dissociative adsorption results in the fast deposition of carbon on the surface while weak H_2 adsorption results in low availability of hydrogen on the surface. Our data can neither prove nor contradict these theories. However, some hypothesis can be done by analyzing the catalyst stability with time on stream. If the K-effect on the deposition of inactive carbon species is the main reason for the decreased catalyst activity at high K-loadings, we expect to observe a progressive catalyst deactivation with time on stream, as a result of the hold-up of carbon on the catalyst. On the contrary, if the K-effects on the competitive adsorption are the main reason for the variation of the catalyst reactivity with K-loading (thermodynamic effect), we expect indeed a low catalyst activity observed immediately after the beginning of the test. Our data point out a complex situation, suggesting that K-loading does affect both the catalyst activation rate and the competitive adsorption of CO and H_2. Indeed, as shown in Fig. 6, cat4K shows an initial activity which is significantly higher than that of cat2K. However, it experiences an important deactivation, which results in a steady tate activity very similar to that of cat2K. Further studies are presently ongoing in out labs to decouple the effects of potassium loading on catalyst activity and stability.

Besides activity, potassium has also a slight effect on the selectivity. As a matter of facts, "cat4K" has a CO_2 selectivity of 32.0%, which has to be compared to 28.8% in the case of "cat2K" (Table 3). Similarly, methane selectivity only slightly increases with the potassium content and the ASF distributions measured with the two catalysts are very similar (cf. Fig. 9 and Fig. 10) as well as the O/P ratio in the products (cf. Fig. 8 and Fig. 11).

Such effects do agree with those reported by Yang et al. [28], who have observed that catalysts with potassium contents similar to those adopted in this paper show similar selectivities. However, other studies reported that K has strong effects on the process selectivity. In fact, other authors observed that upon addition of potassium, the selectivity to heavy products either increases monotonically [43] or it does show a local maximum and then decreases [28,46,47], or stabilizes at high K-contents [28].

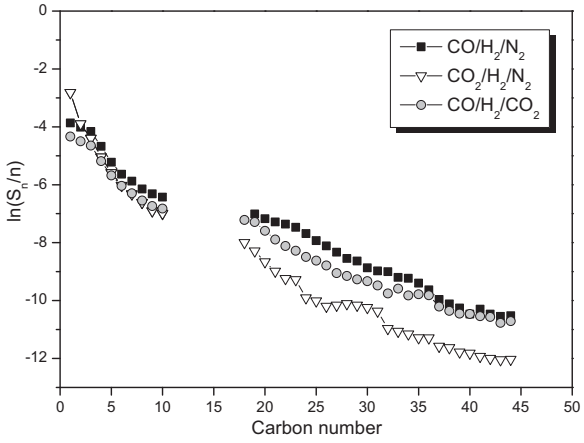

Fig. 10. ASF plots during CO_x hydrogenation ("cat4K", experimental conditions as in Table 2).

3.3.2. *Reactivity of $CO_2/H_2/N_2$*

In the case of CO_2 hydrogenation, the potassium loading does not have any relevant effect on the catalyst activity: CO_2 conversion was found to be 8.3% for "cat4K" and 7.9% for "cat2K" (Table 3). Analogous results were obtained by Prasad et al. [49] over 100Fe/6.6Al/15.7Cu/2–8K catalysts. However, other papers [18,50] report that beneficial effects on the CO_2 conversion rate can be obtained at higher K-loading (up to 0.5 K/Fe molar ratio [51]). At these very high K-loadings, however, in light of the results discussed in Section 3.3.1, the ability of the catalyst to convert CO/H_2 mixtures and also $CO/CO_2/H_2$ mixtures is expected to be very low.

Surprisingly, as opposite to what has been found in the case of CO hydrogenation, potassium has a strong effect on the product selectivity during CO_2 hydrogenation. The CO selectivity increases from 19.5 to 30.3% with increasing K/Fe ratio from 2 to 4 mol.% (Table 3) indicating a strong increase of the reverse-water-gas-shift reaction rate. Methane selectivity also decreases (going from 12.4 to 5.9%), as well as the selectivity to light hydrocarbons (cf. Figs. 9 and 10). This latter aspect is well accounted by the value of the chain growth probability which grows from 0.56 ("cat2K") to 0.67 ("cat4K"). Such effects, which can be assigned to a decrease of the catalyst hydrogenating ability (K promotes CO_2 adsorption, while inhibits H_2 adsorption), are in good agreement with the increase of the O/P ratio (cf. Figs. 8 and 11), which significantly grows when doubling the K-loading of the catalyst.

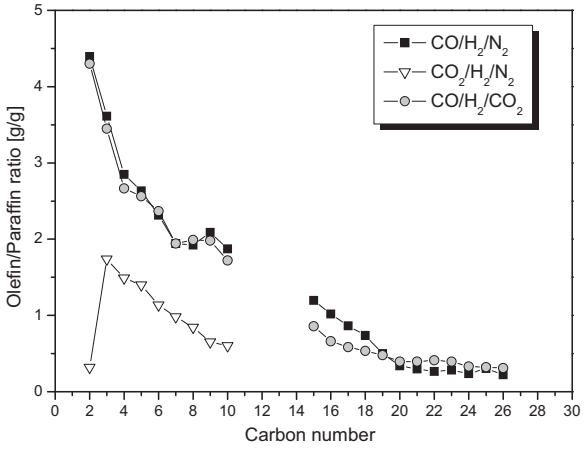

Fig. 11. O/P ratio during CO_x hydrogenation ("cat4K", experimental conditions as in Table 2).

In the range of K/Fe between 2 and 4 wt.%, the effects of potassium are thus extremely different during CO and CO_2 hydrogenation. In fact, potassium suppresses the CO activation rate but does not affect the process selectivity; in the case of CO_2 hydrogenation, K does not affect the catalyst activity but promotes the selectivity to olefins and long chain hydrocarbons.

3.3.3. *Reactivity of $CO/H_2/N_2$ vs. $CO_2/H_2/N_2$ vs. $CO/H_2/CO_2$*

Once verified the effect of the potassium loading for the CO_2 and CO hydrogenation, this effect has been also investigated in the presence of the $CO/H_2/CO_2$/Ar mixture (condition #3 in Table 2). In the case of "cat4K" the CO conversion is about 7.5%, the hydrogen conversion is 22.3% while the CO_2 conversion is 2.1%. Accordingly, as in the case of "cat2K", CO_2 is not significantly consumed nor formed in the presence of CO and its presence does not inhibit the hydrocarbon formation rate. This latter aspect results in paraffin and olefin yield (Fig. 7(d)–(e)) comparable to those found in the case of CO hydrogenation. As a consequence, also the hydrocarbon yield Fig. 7(f) and the ASF product distribution (Fig. 10) are similar to those obtained with the $CO/H_2/N_2$ mixture, as well as the O/P ratio (Fig. 11).

As in the case of "cat2K", it is speculated that the limited CO_2 reactivity is due to the low adsorption ability on the catalyst surface; in the presence of strongly adsorbed CO, which for "cat4K" is even more strongly adsorbed than for "cat2K", CO_2 cannot compete for free catalytic sites. As a result, CO_2 is not adsorbed and it does not react.

The stronger CO adsorption on "cat4K" results also in a decrease of CO conversion with respect to the case of "cat2K" (Table 3); it is known, indeed, that the CO conversion kinetics are negative orders with respect to CO at high CO partial pressure [52], thus reflecting a self-inhibiting effect of this molecule. Also in this case, however, it is not possible to fully decouple the kinetic/thermodynamic effects from those due to catalyst deactivation.

On the contrary, in line with what is observed in the presence of the $CO/H_2/N_2$ mixture, increased K-loading does not affect much the selectivity of the process.

4. Conclusion

The possibility to hydrogenate CO_2 to long chain hydrocarbons, in the presence and in absence of CO, has been investigated in this work over two K- and Cu-promoted iron-zinc catalysts under conditions typical of the low-temperature Fischer–Tropsch, in the presence of H_2-deficient CO_x/H_2 mixtures.

At low K-loadings (K/Fe = 0.02 molar ratio), both CO and CO_2 are readily hydrogenated but the reactivity for CO_2 is around 2 times lower than that of CO. The feed gas composition strongly influences the product selectivity also. In fact, while heavy hydrocarbons up to C_{46} are detected in the product pool in the case of CO hydrogenation; in the case of CO_2 hydrogenation, the main reaction products are light hydrocarbons, especially paraffins. The different reactivity of the two mixtures has been explained considering the relative adsorption strengths of CO, H_2, and CO_2 on the surface which results in very different local H/C ratios able to control the product selectivity. In the case of hydrogenation of CO/CO_2 mixtures, CO_2 behaves as an inert, being characterized by a negligible conversion. Nevertheless, it prevents the CO conversion into CO_2, thus improving the atom efficiency of the process; all the CO converted is transformed into useful hydrocarbons.

At higher K-contents (K/Fe = 0.04 molar ratio), the catalyst ability to hydrogenate CO, CO_2, and their mixtures is modified. In the case of CO and CO/CO_2 hydrogenation, potassium decreases the activity but it has no effect on the product selectivity. On the contrary, when pure CO_2 is hydrogenated, potassium loading does not affect the conversion while it affects the process selectivity by increasing the olefins to paraffins ratio and the average molecular weight of the products.

In conclusion, traditional iron-based catalysts for the Fischer–Tropsch synthesis can be successfully used to obtain high added-value products from CO_2 even in the presence of H_2 deficient feed. The most promising results are obtained with strongly potassium promoted iron catalysts. Nevertheless, a fine tuning of the catalyst formulation is required in order to find the best compromise between activity and selectivity as a function of the desired products and the feed gas composition.

References

[1] K.M.K. Yu, I. Curcic, J. Gabriel, S.C. Tsang, Chem. Sus. Chem. 1 (2008) 893–899.
[2] P. Styring, D., Jansen, H. de Coninck, H., Reith, K., Armstrong, Carbon capture and utilization in the green economy: using CO_2 to manufacture fuel, chemicals and materials. The Centre for Low Carbon Futures 2011, Report number 501. ISBN: 978-0-9572588-1-5.
[3] B. Notari, in: J.M. Thomas, K.I. Thomas (Eds.), Perspectives in Catalysis, Blackwell Scientific Publications, London, 1992.
[4] D.H. Chun, H.-T. Lee, J.I. Yang, H.-J. Kim, J-H. Yang, J.C. Park, B.-K. Kim, H. Jung, Catal. Lett. 142 (2012) 452–459.
[5] W. Wang, S. Wang, X. Ma, J. Gong, Chem. Soc. Rev. 40 (2011) 3703–3727.
[6] J.R. Rostrup-Nielsen, Stud. Surf. Sci. Catal. 81 (1994) 25–41.
[7] P. Kaiser, R.B. Unde, C. Kern, A. Jess, Chem. Ing. Tech. 85 (2013) 489–499.
[8] G.D. Weatherbee, C.H. Bartholomew, J. Catal. 87 (1984) 352–362.
[9] M.K. Gnanamani, W.D. Shafer, D.E. Sparks, B.H. Davis, Catal. Commun. 12 (2011) 936–939.
[10] C.G. Visconti, L. Lietti, E. Tronconi, P. Forzatti, R. Zennaro, E. Finocchio, Appl. Catal. A: Gen. 335 (2009) 61–68.
[11] T. Riedel, M. Claeys, H. Schulz, G. Schaub, S.S. Nam, K.W. Jun, M.J. Choi, G. Kishan, K.W. Lee, Appl. Catal. A: Gen. 186 (1999) 201–213.
[12] Y. Zhang, G. Jacobs, D.E. Sparks, M.E. Dry, B.H. Davis, Catal. Today 71 (2002) 411–416.
[13] Y. Yao, X. Liu, D. Hildebrandt, D. Glasser, Appl. Catal. A: Gen. 433–434 (2012) 58–68.
[14] A.N. Akin, M. Ataman, A.E. Aksoylu, Z.I. Önsana, React. Kinet. Catal. Lett. 76 (2002) 265–270.
[15] G.D. Weatherbee, C.H. Bartholomew, J. Catal. 77 (1982) 460–472.
[16] T. Riedel, G. Schaub, Top. Catal. 26 (2003) 145–156.
[17] D.S. Newsome, Catal. Rev. Sci. Eng. (1980) 21–275.
[18] J.F. Lee, W.S. Chern, M.D. Lee, Can. J. Chem. Eng. 70 (1992) 511–515.
[19] R.A. Fiato, E. Iglesia, G.W. Rice, S.L. Soled, Stud. Surf. Sci. Catal. 114 (1998) 339.
[20] T. Riedel, H. Schulz, G. Schaub, K.-W. Jun, J.-S. Hwang, K.W. Lee, Top. Catal. 26 (2003) 41–54.
[21] Y. Yao, X. Liu, D. Hildebrandt, D. Glasser, Ind. Chem. Res. 50 (2011) 11002–11012.
[22] D.J. Dwyer, G.A. Somorjai, J. Catal. 52 (1978) 291.
[23] H. Ando, Y. Matsumura, Y. Souma, J. Mol. Catal. A: Chem. 154 (2000) 23–29.
[24] L. Xu, S. Bao, D.J. Houpt, S.H. Lambert, B.H. Davis, Catal. Today 36 (1997) 347–355.
[25] S. Li, A. Li, S. Krishnamoorthy, E. Iglesia, Catal. Lett. 77 (2001) 197–205.
[26] A. Kundu, S. Anand, H.C. Verma, Power Technol. 132 (2003) 131–136.
[27] S.R. Yan, K.W. Jun, J.S. Hong, M.J. Choi, K.W. Lee, Appl. Catal. A: Gen. 194 (2000) 63–70.
[28] Y. Yang, H.W. Xiang, Y.Y. Xu, L. Bai, Y.W. Li, Appl. Catal. A: Gen. 266 (2004) 181–194.
[29] N. Lohitharn, J.G. Goodwin, J. Catal. 260 (2008) 7–16.
[30] H. Wan, B. Wu, C. Zhang, H. Xiang, Y. Li, J. Mol. Catal. A: Chem. 283 (2008) 33–42.
[31] M. Liang, W. Kang, K. Xie, J. Nat. Gas. Chem. 18 (2009) 110–113.
[32] G. Munteanu, L. Ilieva, D. Andreeva, Thermochim. Acta 291 (1997) 171–177.
[33] C. Li, Effect of Potassium and Copper Promoters on Reduction Behavior of Precipitated Iron Catalyst, Ph.D Dissertation, Texas A & M University, College Station, 1988.
[34] D.B. Bukur, M. Koranne, X. Lang, K.R.P.M. Rao, G. Huffman, Appl. Catal. A: Gen. 126 (1995) 85–113.
[35] H. Wang, Y. Yang, J. Xu, H. Wang, M. Ding, Y. Li, J. Mol. Catal. A: Chem. 326 (2010) 29–40.
[36] Y. Yang, H.-W. Xiang, L. Tian, H. Wang, C.-H. Zhang, Z.-C. Tao, Y.-Y. Xu, B. Zhong, Y.-W. Li, Appl. Catal. A: Gen. 284 (2005) 105–122.
[37] C.G. Visconti, M. Mascellaro, Catal. Today 214 (2013) 61–73.
[38] C.G. Visconti, Ind. Eng. Chem. Res. (2014), DOI: 10.1021/ie4015638.
[39] S.L. Soled, E. Iglesia, S. Miseo, B.A. DeRites, R.A. Fiato, Top. Catal. 2 (1995) 193–205.
[40] J. Huyser, M.J. van Vuuren, G. Kupi, in: B.H. Davis, M. Occelli (Eds.), Advances in Fischer–Tropsch Synthesis, Catalysts and Catalysis, Taylor & Francis Group, LLC, 2013, pp. 185–197.
[41] T. Herranz, S. Rojas, F.J.P. Aloso, M. Ojeda, P. Terros, J.L.G. Fierro, Appl. Catal. A: Gen. 311 (2006) 66–75.

[42] C.G. Visconti, E. Tronconi, L. Lietti, P. Forzatti, S. Rossini, R. Zennaro, Top. Catal. 54 (2011) 786–800.
[43] D.G. Miller, M. Moskovits, J. Phys. Chem. 92 (1988) 6081–6085.
[44] D.H. Chun, H.T. Lee, J.I. Yang, H.J. Kim, J.H. Yang, J.C. Park, B.K. Kim, H. Jung, Catal. Lett. 142 (2012) 452–459.
[45] W.D. Deckewer, R. Kokuun, E. Sanders, S. Ledakowicz, Ind. Eng. Chem. Process Dev. 25 (1986) 643.
[46] A.P. Raje, R.J. O'Brien, B.H. Davis, J. Catal. 180 (1998) 36–43.
[47] D.B. Bukur, D. Mukesh, S.A. Patel, Ind. Eng. Chem. Res. 29 (1990) 194–204.
[48] H. Kölbel, H. Giehring, Z. Wirkung, Brennstoff-Chem. 44 (1963) 343–369.
[49] P.S.S. Prasad, J.W. Bae, K.W. Jun, K.W. Lee, Catal. Surv. Asia 12 (2008) 170–183.
[50] R.W. Dorner, D.R. Hardy, F.W. Williams, H.D. Willauer, Appl. Catal. A: Gen. 373 (2010) 112–121.
[51] G. Kishan, M.W. Lee, S.S. Nam, M.J. Choi, K.W. Lee, Catal. Lett. 56 (1998) 215–219.
[52] E. Van Steen, H. Schulz, Appl. Catal. A: Gen. 186 (1999) 309–320.